

Articles

Electrokinetic Transport in Nanochannels. 1. Theory

Sumita Pennathur* and Juan G. Santiago

Department of Mechanical Engineering, Stanford University, Stanford, California 94305

Electrokinetic transport in fluidic channels facilitates control and separation of ionic species. In nanometer-scale electrokinetic systems, the electric double layer thickness is comparable to characteristic channel dimensions, and this results in nonuniform velocity profiles and strong electric fields transverse to the flow. In such channels, streamwise and transverse electromigration fluxes contribute to the separation and dispersion of analyte ions. In this paper, we report on analytical and numerical models for nanochannel electrophoretic transport and separation of neutral and charged analytes. We present continuum-based theoretical studies in nanoscale channels with characteristic depths on the order of the Debye length. Our model yields analytical expressions for electroosmotic flow, species transport velocity, streamwise-transverse concentration field distribution, and ratio of apparent electrophoretic mobility for a nanochannel to (standard) ion mobility. The model demonstrates that the effective mobility governing electrophoretic transport of charged species in nanochannels depends not only on electrolyte mobility values but also on ζ potential, ion valence, and background electrolyte concentration. We also present a method we term electrokinetic separation by ion valence (EKSIV) whereby both ion valence and ion mobility may be determined independently from a comparison of micro- and nanoscale transport measurements. In the second of this two-paper series, we present experimental validation of our models.

The advent of well-defined nanoscale fluidic (nanofluidic) channel systems has spurred both speculation and experimentation into their possible applications in the analysis of chemical and biological species.^{1–3} The distinct physical regimes of nanofluidic channel systems offer interesting possibilities for new functionality, including separation and analysis modalities. An effective technique for pumping liquids in such systems is electroosmotic flow. Electroosmotic flow is generated by electric body forces within an electric double layer (EDL) that spontane-

ously forms at solid–liquid interfaces⁴ and whose dimensions scale as the Debye length of the electrolyte.⁵ The counterions of the EDL shield the wall charge within a region that scales with Debye length. In nanoscale channel systems, channel dimensions are of the order of the Debye length, transverse electromigration plays a critical role in determining ion distributions, and a highly nonuniform velocity profile is established.^{6–10}

Analytical studies of potential distributions and electrokinetic transport within long thin channels with significant EDL thicknesses date back at least several decades.^{4,8–22} Since the EDL thickness of typical aqueous electrolytes typically ranges from 1 nm to a theoretical maximum of $\sim 1 \mu\text{m}$,²³ fluidic systems with finite and overlapping double layers can be referred to as nanoscale electrokinetic systems. Burgeen and Nakache⁶ developed theory for electrokinetic flow in capillary slits with finite double layers and predicted a high degree of flow retardation in channel flows having a large Debye length-to-channel height ratio. Their work examines systems with both low and high nondimensional zeta potentials, $\zeta^* = \zeta ze/kT$, where ζ is zeta potential and kT/ze is the thermal voltage.²³ The work of Burgeen and Nakache is well complemented by the work of Levine and co-workers.^{7–9}

- (4) Lyklema, J. *Fundamentals of Interfacial and Colloid Science*, 2; Academic Press: New York, 1995.
- (5) Probstein, R. F. *Physicochemical Hydrodynamics*, 2nd ed.; John Wiley and Sons: New York, 1994.
- (6) Burgeen, D.; Nakache, F. R. *J. Phys. Chem.* **1964**, *68*, 1084–1091.
- (7) Rice, C. L.; Whitehead, R. *J. Phys. Chem.* **1965**, *69*, 417–424.
- (8) Levine, S.; Marriotti, J. R.; Robinson, K. J. *Chem. Soc., Faraday Trans. 2* **1974**, *71*, 136.
- (9) Levine, S.; Marriotti, J. R.; Neale, G.; Epstein, N. J. *Colloid Interface Sci.* **1975**, *52*, 136–149.
- (10) Conlisk, A. T.; Hansford, D. J.; Zheng, Z. *Electrophoresis* **2003**, *24*, 3006–3017.
- (11) Aguilera, V.; Aguilera-Arzo, M.; Ramirez, P. J. *Membr. Sci.* **1996**, *113*, 191–204.
- (12) Conlisk, A. T.; McFerran, J. *Anal. Chem.* **2002**, *74*, 2139–2150.
- (13) Daiguji, H.; Yang, P.; Majumdar, A. *Nano Lett.* **2004**, *4*, 137–142.
- (14) Datta, R.; Kotamurthi, V. R. *AIChE J.* **1990**, *36*, 916–926.
- (15) Datta, B.; McEldoon, J. P. *Anal. Chem.* **1992**, *64*, 227–223.
- (16) Dutta, P.; Beskok, A. *Anal. Chem.* **2001**, *73*, 1979–1986.
- (17) Griffiths, S.; Nilson, R. H. *Anal. Chem.* **1999**, *71*, 5522–5529.
- (18) Griffiths, S.; Nilson, R. H. *Anal. Chem.* **2000**, *72*, 4767–4777.
- (19) Hildreth, D. *J. Phys. Chem.* **1969**, *74*, 2006–2015.
- (20) Kuo, T.-C.; Sloan, L. A.; Shannon, M. A.; Sweedler, J. V.; Bohn, P. W. *Sens. Actuators, A* **2003**, *102*, 223–233.
- (21) Qiao, R.; Aluru, N. R. *Phys. Rev. Lett.* **2004**, *92*, 1–4.
- (22) Qiao, R.; Aluru, N. R. *Int. J. Multiscale Comput. Eng.* **2004**, *2*, 173–188.
- (23) Hunter, R. J. *Zeta Potential in Colloid Science: Principles and Applications*; Academic Press: New York, 1981.

* To whom correspondence should be addressed. E-mail: sumita@stanford.edu. Fax: (650)-723-7657.

- (1) Li, W.; Tegenfeldt, J. O.; Chen, L.; Austin, R. H.; Chou, S. Y.; Kohl, P. A.; Krotine, J.; Sturm, J. C. *Nanotechnology* **2003**, *14*, 578–583.
- (2) Slavik, G. J. *NINN REU Res. Accomplishments* **2004**, 124–125.
- (3) Quake, S. R.; Scherer, A. *Science* **2000**, *290*, 1536–1540.

Collectively these seminal papers are limited to liquid velocity fields and net current transport and do not address the transport of individual, charged solute species over long distances (i.e., electrophoresis). Other, more recent examples of electrokinetic flow theory development include work on combined pressure-driven flow and (streamwise) electrophoretic ion motion,¹⁴ the effects of adsorption/desorption dynamics on electrophoresis,^{15,24} and the dispersion dynamics of neutral solutes in electrokinetic nanochannels.^{17,18} Although a few of these studies investigate the migration of individual species,^{14,15,17,18,24} none of them address the role of coupling between transverse and streamwise electromigration fluxes and the effect of this coupling on electrophoresis and analyte dispersion. Also, most of the studies are restricted to the assumption of low ζ potential.^{14,15,17,24}

There are a few recent experimental studies of molecular transport through planar, shallow nanochannels.^{11,25–31} Shu et al.³¹ fabricated nanochannels for the application of stretching and studying the dynamics of 103-kbase T5 phage DNA. Petersen et al.²⁸ fabricated nanochannels for DNA separation and demonstrated a separation between strand lengths of 100 and 1000 base pairs in a 320-nm-deep channel. Stein et al.³⁰ performed experiments in nanochannels to quantify the effects of surface charge on net ion transport. The latter study measured total ion current as a function of bulk conductivity (i.e., electrolyte conductivity measured outside of channel) in 70-nm and 1.015- μm channels with λ_D ranging from 0.3 to 100 nm. Pu et al.²⁶ qualitatively described an ion depletion effect at the interface between nano- and microchannels. Image intensity data were recorded for 60-nm-deep channels with electrolyte concentrations of 70 μM , and ion depletion was characterized with 30 μM fluorescein in unbuffered solutions. Although a few of these experimental studies examined the effects of individual species,^{26,28,32} none addressed electrophoretic transport of individual charged species and its coupling with transverse electromigrative fluxes.

Table 1 summarizes typical examples of theoretical and experimental studies of electrokinetic flow in systems with a finite EDL. We use symbols to summarize the content of each paper. For the theoretical work, they are as follows: u are studies of liquid velocity fields; $\zeta^* > 1$ denotes theory with a validity extending in the high ζ potential regime; $N > 1$ denotes investigations of distribution of multiple ions in the EDL; κ_S are studies of surface conductivity effects;³³ c_i denotes studies of the transport of individual neutral species; and the symbol zc_i is used to denote transport of charged species. For the experimental work, they are as follows: I denotes measurements of total ion current; u are experimental measurements of liquid transport; and c_i are measurements of the transport of individual (charged or uncharged) species.

- (24) Martin, M.; Guiochon, G. *Anal. Chem.* **1984**, *56*.
 (25) Martin, C. R.; Mishizawa, M.; Jirage, K. B.; Kang, M. J. *Phys. Chem. B* **2001**, *105*, 1925–1934.
 (26) Pu, Q.; Yun, J.; Temkin, H.; Liu, S. *Nano Lett.* **2004**, *4*, 1099–1103.
 (27) Tas, N. R. *J. Micromech. Microeng.* **1996**, *6*, 385.
 (28) Petersen, N.; Alarie, J. P.; Ramsey, J. M., Squaw Valley, CA; Northrup, A. 2003; pp 701–703.
 (29) Jacobson, S. C.; Moore, A. W.; Ramsey, J. M. *Anal. Chem.* **1995**, *67*, 2059–2063.
 (30) Stein, D.; Kruthof, M.; Dekker, C. *Phys. Rev. Lett.* **2004**, *93*, 1–4.
 (31) Shu, D.; Moll, W. D.; Deng, Z.; Mao, C. *Nano Lett.* **2004**, *69*–73.
 (32) Guo, ? *Nano Lett.* **2004**, *4*, 69–73.
 (33) Lyklema, J. *J. Phys.: Condens. Matter* **2000**, *13*, 5027–5034.

Table 1. Theoretical and Experimental Nanochannel Electrokinetic Studies

reference	theory	experiments
Burgeon and Nakache ⁶	$\zeta^* > 1, u$	
Rice and Whitehead ⁷	u	
Levine et al. ⁸	$\zeta^* > 1, u$	
Qiao and Aluru ²²	$\zeta^* > 1, N > 1, u, \kappa_S$	
Griffiths and Nilson ¹⁸	$\zeta^* > 1, u, c_i$	
Martin et al. ²⁴	κ_S, c_i	
Datta and McEldoon ¹⁵	u, c_i	
Griffiths and Nilson ¹⁷	u, c_i	
Daiguji et al. ¹³	$\zeta^* > 1, \kappa_S, N > 1$	
Datta and Kotamurthi ¹⁴	u, c_i	
Stein et al. ³⁰	κ_S	I, u
Guo et al. ³²	u, c_i	c_i
Pu et al. ²⁶	$N > 1, c_i$	I, c_i
Fang et al. ³⁴	c_i	c_i
Peterson et al. ²⁸	u, c_i	u, c_i
current work	$u, \zeta^* > 1, zc_i$	
Pennathur and Santiago ³⁵		u, I, c_i

In this paper, we present theory valid for electrokinetic transport in nanometer-scale channels. We study electrophoretic transport of both charged and neutral species in long thin nanochannels and show that both transverse electromigration and nonuniform velocities have a significant effect on both net streamwise transport and dispersion. We present continuum theory valid for the finite ζ^* regime and Debye lengths on the order of the channel height. We also present a method we term electrokinetic separation by ion valence (EKSIV) that can be used to determine both ion mobility and valence of analyte ions from a comparison of micro- and nanoscale transport measurements. In the second of this two-paper series,³⁵ we present an experimental validation of the model.

CONTINUUM THEORY MODEL

Liquid Transport Simulations. We first summarize the governing equations for transport of liquids in channel flows where λ_D is on the order of at least one characteristic channel dimension. We begin with the classical equations describing electrokinetic flows, as presented by Levich³⁶ and Probstein.⁵ Assuming fully developed flow and negligible flow to pressure gradients, the continuum equations are

$$\nabla \cdot \bar{u} = 0; \quad 0 = \mu \nabla^2 \bar{u} + \rho_e \nabla \Phi \quad (1)$$

$$\nabla^2 \Phi = \frac{-\sum_{i=1}^N z_i e n_c \exp(-z_i e \Phi / kT)}{\epsilon} \quad (2)$$

where \bar{u} is the velocity of the liquid, ρ_e is the charge density, μ is the viscosity, ϵ is the permittivity, e is the elementary charge, k is the Boltzmann constant, T is temperature, z is valence number, and n_c is the number density (m^{-3}) in the center of the channel for a channel with nonoverlapped EDLs. Equations 1 are the

- (34) Fang, C.; Wu, B.; Zhou, X. *Electrophoresis* **2004**, *25*, 375–380.
 (35) Pennathur, S.; Santiago, J. *Anal. Chem.* **2005**, *77*, 6782–6789. ac0508346
 (36) Levich, V. G. *Physicochemical Hydrodynamics*; Prentice-Hall: Englewood Cliffs, NJ, 1962.

equations of motion for an incompressible Newtonian fluid of uniform viscosity subject to an electrostatic body force. Equation 2 is the Poisson–Boltzmann equation relating electric potential and electrolyte ion distributions in the channel.

Following Probst, ⁵ we decompose the electrical potential in the system as follows (in Cartesian coordinates):

$$\Phi = \phi(x) + \Psi(y,z) \quad (3)$$

where Φ is the total potential in the channel, ϕ is the external potential imposed by end-channel electrodes, and Ψ is the potential field associated with the charges of the EDL.

Assuming an electric body force term induced by the charges of a uniform ζ potential, eq 1 can be integrated to yield

$$u(y,z) = -\frac{\epsilon E \zeta}{\mu} \left(1 - \frac{\psi(y,z)}{\zeta} \right) \quad (4)$$

where u is the streamwise component of velocity, E is the streamwise electric field induced by the end-channel electrodes, x is the streamwise direction, and y and z are respectively the transverse and spanwise directions. We approximate the net charge density distribution as being only a function of the EDL potential, ψ , described by eqs 2. Note that area-averaged velocities, $\langle u \rangle$, are of the form

$$\langle u \rangle = \frac{1}{4wh} \int_{-h}^h \int_{-w}^w \frac{\epsilon E \zeta}{\mu} \left(1 - \frac{\psi(y,z)}{\zeta} \right) dy dz \quad (5)$$

We solved these equations numerically for finite ζ^* using a commercially available finite element solver (FEMLAB, Comsol Corp., Los Angeles, CA) with the incompressible Navier–Stokes and dc conductive media application modules. The three-dimensional (3D) channels geometries (and associated 2D flow simulations) incorporated a 20:1 width-to-depth aspect ratio consistent with our experiments. ³⁵ The viscosity and permittivity of the dilute electrolyte are those of water, 9.77×10^{-4} kg/ms and 6.93×10^{-10} C²/J·M, respectively. ³⁷ Note that we assume viscosity and permittivity are uniform and constant within the double layer, although there may be variability of both these parameters in the EDL, as discussed in detail by Lyklema. ³⁸ We consider electric fields, ζ potentials, and Debye length-to-channel height ratios consistent with experiments, ³⁵ where Debye length is defined as

$$\lambda_D = (\epsilon kT / e^2 \sum_{i=1}^N z_i^2 n_i)^{1/2} \quad (6)$$

For finite ζ^* values, we also used the elliptic integral formulation of Burgeen and Nakache. ⁶ The 1D semianalytical solutions for symmetric electrolytes match the 2D numerical flow simulations at the spanwise midplane ($z = 0$) (also for the symmetric electrolyte case) within 1.5% for Debye length-to-channel height ratios (λ_D/h) between 0 and 0.5. The 1D flow solution is sufficient

(37) Pottel, R. In *Water: A Comprehensive Treatise*; Franks, F., Ed.; Plenum: New York, 1973; Vol. 3, pp 420–423.

(38) Lyklema, J.; Overbeek, J. G. J. *Colloid Sci.* **1961**, *16*, 501–512.

for symmetric analytes in 20:1 aspect ratio channels with finite double layers. For the remainder of this paper, we shall estimate the velocity vector field (u) and potential field (ψ) as functions of only the transverse dimension (y) in the case of high aspect ratio channels (i.e., we treat the flow as between large parallel plates).

Note that for low ζ^* values, the analytical solution for u is derived simply using Debye–Huckel theory ⁵ as

$$u(y) = -\frac{\epsilon E \zeta}{\mu} \left(1 - \frac{A_1 \exp(y/\lambda_D) + A_2 \exp(-y/\lambda_D)}{\zeta} \right) \quad (7)$$

where

$$A_1 = \zeta \frac{1 - \exp(2h/\lambda_D)}{\exp(h/\lambda_D) - \exp(-3h/\lambda_D)}$$

$$A_2 = \zeta \exp(-h/\lambda_D) - A_1 \exp(-2h/\lambda_D)$$

Last, we note that area-averaged (bulk) velocities are a function of the nondimensional velocity profile (as determined by ζ^*). ¹⁸ Measurable area-averaged velocities therefore hold information regarding the shape of the EDL.

Regular Perturbation Theory. Considering a system of three fully ionized ions, A, B, and S, where ions A and B represent the influence of all background electrolytes and S is the analyte ion. Ion transport is governed by the following electromigration–diffusion–advection equation. ³⁹

$$\frac{\partial c_i}{\partial t} + \bar{u} \cdot \nabla \bar{c}_i = +z_i \nu_i F \bar{\nabla} \cdot (c_i \nabla \bar{\Phi}) + D_i \nabla^2 c_i; \quad i = A, B, S \quad (8)$$

where c_i refers to the concentration of the i th ionic species, (e.g., c_S refers to concentration of sample ion S), F is Faraday's constant, and D is the (isotropic) molecular diffusion coefficient. ν_i is the usual ion mobility of a species defined as a positive quantity equal to u_d / EFz_i , where u_d is the net velocity (i.e., relative to the local liquid velocity) for an ion valance z_i subject to an electric field E . We follow the regular perturbation analysis of Bharadwaj and Santiago ³⁹ and find that the zeroth order equations show that background electrolyte ions follow binary electrolyte dynamics and are unaffected by the convection, diffusion, and electromigration of the relatively low concentration analyte (sample concentration should be lower than about one-tenth of the background electrolyte ion concentration). Following this procedure, the first-order low concentration sample analyte ion distribution is

$$\frac{\partial c_S^1}{\partial t} + \bar{u}^0 \cdot \nabla \bar{c}_S^1 = z_S \nu_S F \bar{\nabla} \cdot (c_S^1 \nabla \bar{\Phi}^0) + D_S \nabla^2 c_S^1 \quad (9)$$

From eq 9, we see that the sample ion concentration is a first-order concentration field that responds as a passive (although charged and diffusive) scalar to the velocity and electric fields determined by the zero-order background electrolyte ions. For the remainder of this paper, we will focus on the behavior of this

(39) Bharadwaj, R.; Santiago, J. Submitted to *Anal. Chem.*

first-order sample ion concentration field and will, for brevity, omit the superscript 1 from subsequent equations.

Time Scale Analysis. We now use a straightforward time scale argument to derive a transverse concentration distribution at any streamwise location x . For two-dimensional (xy) concentration fields in a one-dimensional flow parallel to the x -axis, eq 9 can be rewritten as follows:

$$\frac{\partial c_S}{\partial t} + (u^0 + v_S z_S F E_x) \frac{\partial c_S}{\partial x} = v_S z_S F \frac{d\psi}{dy} \frac{\partial c_S}{\partial y} + v_S z_S F c_S \frac{d^2 \psi}{dy^2} + D \left(\frac{\partial^2 c_S}{\partial x^2} + \frac{\partial^2 c_S}{\partial y^2} \right) \quad (10)$$

where c_S is the concentration of the species ion with an electromigration determined by the analyte ion mobility, v_S . The electric potential has been expanded as

$$\nabla \Phi^0 = \frac{d\phi}{dx} \bar{i} + \frac{d\psi}{dy} \bar{j} = -E_x \bar{i} + \frac{d\psi}{dy} \bar{j} \quad (11)$$

where the applied electric field (E_x) is uniform and constant. We now apply a normalization of the form

$$t^* = \frac{t}{t_0}, \quad c^* = \frac{c_S}{c_{S0}}, \quad x^* = \frac{x}{\sigma_0}, \quad y^* = \frac{y}{\lambda_D}, \quad \frac{d\psi^*}{dy^*} = \frac{d\psi}{dy} \frac{\zeta}{\lambda_D} \quad (12)$$

where t_0 is the characteristic time scale of an electrophoretic separation, c_{S0} is a characteristic sample concentration, and σ_0 is the characteristic streamwise length of the sample plug (e.g., the width of an analyte band in an electrophoretic separation). In the cases of interest, λ_D is of order h . Further, the maximum velocity (and the scale u^0) is determined solely by the effects of viscous and electrostatic forces,⁴⁰ so the characteristic velocity u^0 is simply $u_{HS} = \epsilon E \zeta / \mu$, the area-averaged velocity expected in a thin EDL flow.⁵

Equation 10 becomes

$$\frac{\lambda_D^2}{Dt_0} \frac{\partial c^*}{\partial t^*} + \frac{u_{HS}(1 + \beta)}{D} \frac{\lambda_D^2}{\sigma_0} \frac{\partial c^*}{\partial x^*} = \zeta^* \frac{\partial \psi^*}{\partial y^*} \frac{\partial c^*}{\partial y^*} + \zeta^* \frac{\partial^2 \psi^*}{\partial y^{*2}} c^* + \frac{\lambda_D^2}{\sigma_0^2} \frac{\partial^2 c^*}{\partial x^{*2}} + \frac{\partial^2 c^*}{\partial y^{*2}} \quad (13)$$

where β is the ratio of ion mobility to the Helmholtz–Smoluchowski EOF velocity, $\mu v_S z_S F / \epsilon \zeta$. Here we have used the Nernst–Einstein relation,⁵ $D = v_S RT$, so $v_S z_S F \zeta / D = z_S e \zeta / kT$. The relevant time scales are $t_{diff} = \lambda_D^2 / D$, $t_{em} = \lambda_D^2 / (\zeta^* D)$, and $t_{adv} = \sigma_0 / u_{HS}$. These scales describe respectively the characteristic times of diffusion in the transverse direction, electromigration in the transverse direction, and the time for the analyte band to advect (i.e., due to area-averaged liquid velocity only) along the streamwise direction a distance on the order of its width.

The characteristic length scales of the problem are $\lambda_D = 10$ nm and $\sigma = 10$ μ m. Characteristic values of other key parameters

are $D = 1 \times 10^{-10}$ m²/s, $E = 100$ V/cm, and $v_S z_S F = 1 \times 10^{-8}$ m²/(V·s). For typical nanoscale systems, ζ^* is of order of unity.²³ Using these values, we find that t_{diff} and t_{em} are on the order 1×10^{-6} s and that both t_{diff} and t_{em} are much smaller than t_{adv} , which is on the order 0.1 s. In terms of the parameters of eq 13, ζ^* is of order unity, while both λ_D^2 / σ_0^2 and $u_{HS}(1 + \beta) \lambda_D^2 / (D \sigma_0)$ are much smaller than unity. We can therefore assume that transverse electromigration (first and second terms on the right-hand side of eq 13) continuously balances transverse concentration gradients (last term of eq 13). This leads to a quasi-steady equilibrium between transverse electromigration and transverse diffusion expressed as

$$0 \cong v_S z_S F \frac{\partial}{\partial y} \left(c_S \frac{\partial \psi}{\partial y} \right) - D \frac{\partial^2 c_S(x, y, t)}{\partial y^2} \quad (14)$$

Equation 13 (and therefore 14) is subject to the following boundary conditions:

$$\psi(y) \rightarrow \psi_c(y) \quad \text{at} \quad y = 0$$

$$c_S(x, y) \rightarrow c_{S,c}(x) \quad \text{at} \quad y = 0$$

where $c_{S,c}(x)$ above is the concentration of sample species at the centerline of the channel and at some arbitrary streamwise position x and ψ_c is the potential at the center of the channel determined by the solutions to eqs 1 and 2.⁶ The transverse height of the channel varies from $y = -h$ to h and eq 14 can be integrated twice to yield

$$c_S(x, y) \cong c_{S,c} \exp\left(\frac{-z_S e (\psi(y) - \psi_c)}{kT}\right) \quad (15)$$

Here $c_{S,c}(x)$ can be related to the area-averaged concentration $\langle c_S \rangle$ at an any streamwise location by the following relation:

$$\langle c_S(x, y) \rangle \cong c_{S,c} \left\langle \exp\left(\frac{-z_S e (\psi(y) - \psi_c)}{kT}\right) \right\rangle \quad (16)$$

where the operator $\langle \rangle$ represents a transverse (y -direction) depth-averaged quantity, $\langle \rangle = 1/(2h) \int_{-h}^h (\cdot) dy$. Since we are estimating the velocity field, u , and potential field, ψ , as functions of only the transverse dimension, y , this operator also represents an area-averaged quantity and will be referred to as such for the remainder of the paper.

Analytical Solution for Charged Species Transport. In this section, we derive closed-form analytical solutions to both the transport and dispersion of charged species using the convective diffusion equation. First, we substitute the transverse concentration distribution for arbitrary streamwise locations (eq 15) into the full convective–diffusion–electromigration equation (eq 10), to yield

$$\exp\left(\frac{-z_S e (\psi(y) - \psi_c)}{kT}\right) \frac{\partial c_{S,c}}{\partial t} + \exp\left(\frac{-z_S e (\psi(y) - \psi_c)}{kT}\right) (u_{HS} - v_S z_S F E_x) \frac{\partial^2 c_{S,c}}{\partial x^2} \cong$$

(40) Santiago, J. *Anal. Chem.* **2001**, *73*, 2353–2365.

$$D \exp\left(\frac{-z_S e(\psi(y) - \psi_c)}{kT}\right) \frac{\partial^2 c_{S,c}}{\partial x^2} \quad (17)$$

Note the first two terms on the left-hand side of eq 10 cancel the last term on the right-hand side of eq 10, as dictated by the fast dynamics of the equilibrium between transverse diffusion and transverse electromigration

Next, we consider a shift of reference frame that will yield a quasi-steady solution of the two-dimensional concentration field in a formulation that is analogous to that originally made by Taylor⁴¹ for quasi-steady dispersion of neutral solutes in pressure-driven flows. Three important differences of the current case from that of Taylor are as follows: both electroosmotic velocity profiles and streamwise electromigration play a role in determining the appropriate reference frame for the current problem; the reference frame velocity in the current problem is at first unknown; and the flux of solute along the transverse direction is here determined by both diffusion and electromigration.

We define the velocity of the quasi-steady reference as the observed velocity of the analyte, $\langle u_S \rangle$ (i.e., the effective velocity of the electrophoretic band with respect to the channel wall). We then integrate eq 17 in y and to obtain area-averaged quantities. Defining $G = \langle \exp(-z_S e\psi(y)/kT) \rangle$, eq 17 becomes

$$G \frac{\partial^2 c_{S,c}}{\partial t} + \left\langle \exp\left(\frac{-z_S e(\psi(y) - \psi_c)}{kT}\right) (u_{HS} - v_S z_S FE_x - \langle u_S \rangle) \right\rangle \frac{\partial^2 c_{S,c}}{\partial x} \cong DG \frac{\partial^2 c_{S,c}}{\partial x^2} \quad (18)$$

Here the bracketed term multiplying the streamwise derivative of centerline concentration is a constant. We recognize that eq 18 has the form of a simple one-dimensional diffusion problem with a shift in reference frame given by a uniform, steady velocity. The only value of $\langle u_S \rangle$ for which the frame of reference moves exactly with the electrophoretic band can be derived by setting the bracketed term in eq 18 to zero to yield

$$\langle u_S \rangle = \frac{\epsilon E \zeta}{\mu} \left\langle \exp\left(\frac{-z_S e(\psi(y) - \psi_c)}{kT}\right) \left(1 - \frac{\psi(y)}{\zeta}\right) \right\rangle + v_S z_S FE \quad (19)$$

Equation 19 defines the observed, area-averaged velocity of a charged species in nanochannel electrokinetic flow. The exponential term describes the transverse distribution of the sample as determined by analyte valence, z_S , and the transverse potential distribution $\psi(y)$ (whose shape is a function of ζ^*). The product of this exponential with $(1 - \psi/\zeta)$ captures the coupling between transverse electromigration and diffusion with streamwise advection. Figure 1 shows a plot of $\langle u_S \rangle$ as a function of λ_D/h for two values of ζ^* and sample ion valences, z_S , of -1 , -2 , 0 , 1 , and 1 . To highlight the transverse electromigration/streamwise flow coupling, we normalize $\langle u_S \rangle$ by first subtracting the electrophoretic component, $v_S z_S FE$, and then dividing by u_{HS} . The figure shows

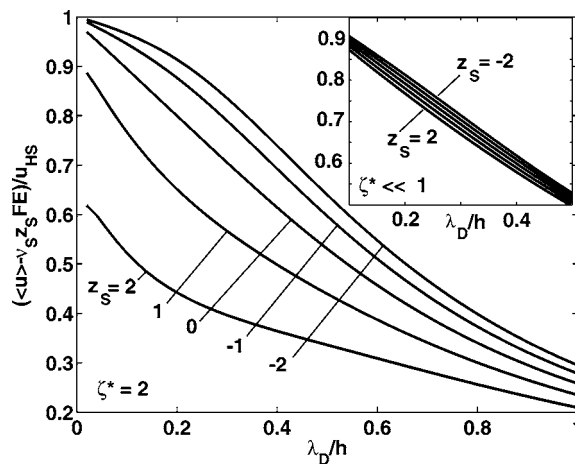


Figure 1. Area-averaged, observable species velocity, $\langle u_S \rangle$, as a function of λ_D/h for $\zeta^* \ll 1$ (insert) and $\zeta = 2$ and for sample ion valences, z_S , of -1 , -2 , 0 , 1 , and 1 . $\langle u_S \rangle$ is normalized by first subtracting the electrophoretic component, $v_S z_S FE$, and then dividing by u_{HS} . The figure shows how positively charged analyte molecules equilibrate close to the channel walls and experience lower liquid velocities. Negative sample ions equilibrate toward the center of the channel and are advected by the higher velocities near the center of the channel.

how positively charged analyte molecules spend relatively more time near the wall and experience lower liquid velocities. Negative sample ions are repelled from the wall and advected by the higher velocities near the center of the channel.

With the definition of $\langle u_S \rangle$ given by eq 19, eq 18 reduces to

$$\frac{\partial c_{S,c}}{\partial t} \cong D \frac{\partial^2 c_{S,c}}{\partial x^2} \quad (20)$$

which, for an initial thin sample injection plug, can be solved exactly to yield a Gaussian function in x for $c_{S,c}$. Note that in our case of interest, where h is order λ_D , the effective dispersion coefficient of the solute is just the molecular diffusion coefficient D . That is, a quasi-steady equilibrium between transverse electromigration and diffusion dictates that advective dispersion cannot, to first order, contribute to streamwise dispersion. Note that the current derivation does not account for adsorption/desorption dynamics, which may also contribute to dispersion. Shifting back to the original reference frame, and substituting for $c_{S,c}$ using eq 15, we can solve for the final concentration distribution in a nanochannel:

$$c_S(x,y,t) = \frac{n_0}{wh} \frac{\exp(-(x - \langle u_S \rangle t)^2 / 4Dt)}{\sqrt{4\pi Dt}} \times \exp\left(\frac{-z_S e(\psi(y) - \psi_c)}{kT}\right) \quad (21)$$

where n_0 is the number of moles of the analyte introduced in the channel and $\langle u_S \rangle$ and $\psi(y)$ are defined by eqs 19 and 2, respectively

(41) Taylor, G. I. *Proc. R. Soc. London, Ser. A* **1953**, *219*, 186–203.

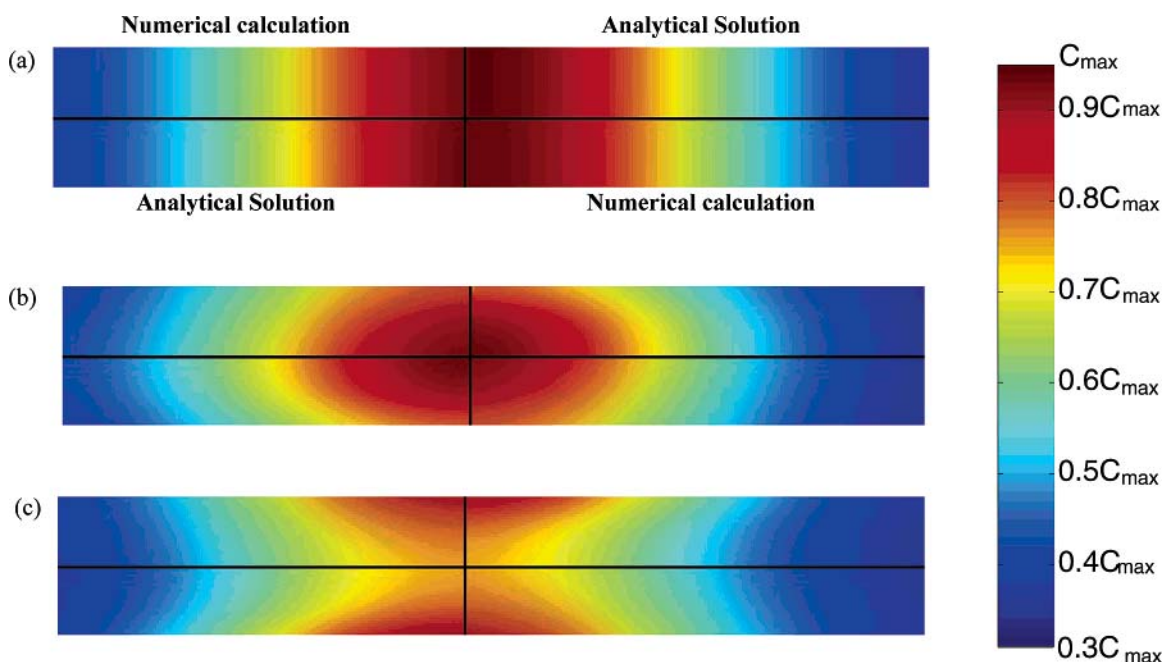


Figure 2. Comparison between analytical solution and numerical calculations of streamwise-transverse concentration fields for convective-diffusion dynamics in nanometer-scale electrokinetic channels. Figure shows (a) a neutral species, (b) a species with a $z_s = 1$ valence number, and (c) a species with a $z_s = -1$ valence number. The analytical concentration fields are shown in the first and third quadrants of each field plot, while numerical results are shown in the second and fourth quadrants. All calculations are for a 50-nm-deep channel with a 6-nm Debye layer thickness and $\zeta^* = 2.1$. Red regions indicate high solute concentration.

Note that for low ζ potential magnitudes, the solution to eq 21 is expressible in closed form:

$$\frac{n_0 \exp(-(x - \langle u_s \rangle t)^2 / 4Dt)}{wh \sqrt{4\pi Dt}} \times \exp\left(\frac{-z_s e (A_1 \exp(y/\lambda_D) + A_2 \exp(-y/\lambda_D))}{kT}\right) \quad (22)$$

Equations 19, 21, and 22 are presented in Appendix A for a cylindrical nanochannel.

Validation of Analytical Solution with Simulations. We here present a validation of our analytical solution with a numerical calculation. We consider the coupled advection and diffusion of a solute band that is initially thin compared to the channel dimension and uniformly distributed in y . We chose an integration time step for this calculation of order $0.1 \lambda_D^2/D$. The numerical calculations can be summarized in three brief descriptions. First, we find that the solute relaxes to a transverse distribution determined by the exact analytical solution within a time scale of order λ_D^2/D , as predicted by the time scale argument presented earlier. Second, over electrophoretic migration times of order $100\lambda_D^2/D$ and greater, the peak concentration of the electrophoretic band moves at a velocity determined by eq 19. In all cases, velocities predicted by eq 19 matched those of the 2D unsteady calculations within 6%. Third, over electrophoretic migration times of order λ_D^2/D and greater, the simulated electrophoretic band reaches an unsteady, 2D distribution well approximated by eq 21, as shown in Figure 2 and discussed below.

Figure 2 shows a comparison between our analytical solution and numerical calculations for both neutral and charged analytes. Streamwise-transverse concentration distributions for neutral,

positively charged, and negatively charged sample species are shown at an integration time of $100\lambda_D^2/D$. Note that the analytical concentration fields are shown in the first and third quadrants of each field, while the numerical results are shown in the second and fourth quadrants. The solutions are calculated in channels with a height of 50 nm, λ_D/h of 0.25, and a sample species diffusion coefficient, D , of $5 \times 10^{-10} \text{ m}^2/\text{s}$. Since we are interested in the regime of nonoverlapped EDLs, both numerical calculations and analytical solutions are presented for the case where ψ_c is negligible. The figure shows excellent agreement between the analytical solution and numerical calculation for both the area-averaged velocity and dispersion. The neutral species solution of Figure 2a is consistent with the low Peclet number limit identified by Griffiths and Nilson¹⁷ for neutral solutes in finite EDL electrokinetic flows. In Figure 2b, the fluxes of electromigration (away from the wall for a negative ion and negative wall charge) and diffusion result in an equilibrium ion distribution where negative ions are concentrated near the center of the channel and experience a velocity higher than that of the area-averaged (bulk) liquid velocity. The opposite is true of the positive analyte ions of Figure 2c, which equilibrate near the wall and experience relatively low liquid velocities. Parts b and c of Figure 2 validate the accuracy of the quasi-steady equilibrium formulation that leverages the fast dynamics of transverse electromigration and diffusion in a nanochannel. In all cases, numerical calculation values of the unsteady, two-dimensional concentration fields are within 3% of the analytical equation (using a simple, trapezoidal numerical integration of $\psi(y)$). Note that the streamwise dispersion for charged species is also consistent with pure streamwise diffusion, $\sigma = (2Dt)^{1/2}$, where σ is variance of width of the sample plug.

Nanochannel Electropherogram Predictions. As a further demonstration of the model, Figure 3 shows spatial electrophero-

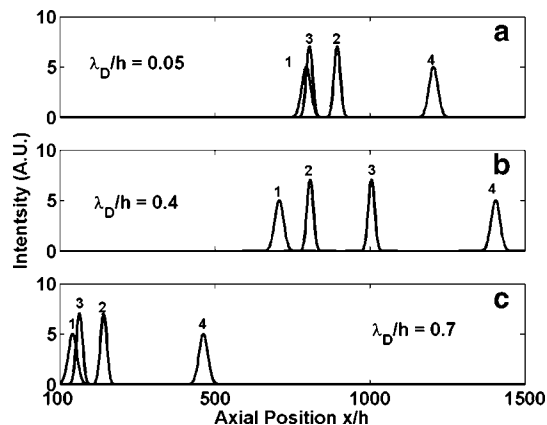


Figure 3. Simulated spatial electropherograms are shown for four analytes separated at a field of 200 V/cm in a channel with $\zeta^* = -2$. The sample analytes in this simulation have the following properties: $\nu_1 = 4 \times 10^{-4}$ mol·s/kg ($z_1 = -1$), $\nu_2 = 1.2 \times 10^{-4}$ mol·s/kg ($z_2 = 1$), $\nu_3 = 2 \times 10^{-4}$ mol·s/kg ($z_3 = -2$), and $\nu_4 = 4 \times 10^{-4}$ mol·s/kg ($z_4 = 1$). Species 1 and 3 have identical values of $z_S \nu_S$ and so migrate at the same rate at thin EDL conditions, $\lambda_D/h = 0.05$ (a). At $\lambda_D/h = 0.4$ (b), the coupling between transverse concentration distributions and the nonuniform velocity field results in an optimal separation rate between species 1 and 2. With relatively thick EDLs, $\lambda_D/h = 0.7$ (c), separation of all species is achieved but with lower resolution.

gram simulations (i.e., plots of area-averaged species concentration versus axial distance at equal times after injection) for three sample values of nondimensional Debye length: $\lambda_D/h = 0.05, 0.4$, and 0.7 . We assume a negative wall charged surface with $\zeta^* = -2$ in all cases. The concentration distributions of each analyte is obtained using eq 21 and plotted independently. Sample analyte anions, species 1 and 3, have the same electrophoretic drift velocity, $z_S F E \nu_S$, but valences of $z_1 = -1$ and $z_3 = -2$. Analyte cations 2 and 4 have equal valence, $z_2 = z_4 = 1$, but species 2 has a lower ion mobility than species 4, $\nu_2 < \nu_4$. Figure 3a shows an electropherogram at thin EDL conditions. Here, species 1 and 3 are unresolved as expected (since $z_1 \nu_1 = z_3 \nu_3$), while species 2 and 4 are resolved by their different mobilities. Figure 3b shows results at $\lambda_D/h = 0.41$, where the separation of species 1 and 3 is most sensitive to ion valence. Here, the coupling between the nonuniform velocity field and nonuniform concentrations in the transverse direction results in clear resolution of all species. At this condition, the order of elution of analytes 2 and 3 is reversed from that of the other two cases. This is again a result of the complex coupling between valence and ion mobility in a finite EDL channel system. Figure 3c shows a separation for a relatively thick, nonoptimal value of $\lambda_D/h = 0.7$. Here, the effectiveness of nanochannel separation decreases as sample analytes are distributed more uniformly over the cross section of the channel and analyte transport is determined mostly by the area-averaged liquid velocity. Also, at this thick EDL condition, $\langle u \rangle$ is relatively low, and so the observed species velocities of the analytes, $\langle u_S \rangle$, are significantly lower than the corresponding velocities of Figure 3a and b. These results demonstrate the efficacy of using nanochannel electrophoretic separations to obtain new ion information. In the next section, we present a method whereby comparisons of micro- and nanoscale electrophoretic separations (e.g., Figure 3a and b above) can be used to obtain both ion mobility and valence.

Effective Electrophoretic Mobility in a Nanochannel: Electrokinetic Separation by Ion Valence.

In this section, we

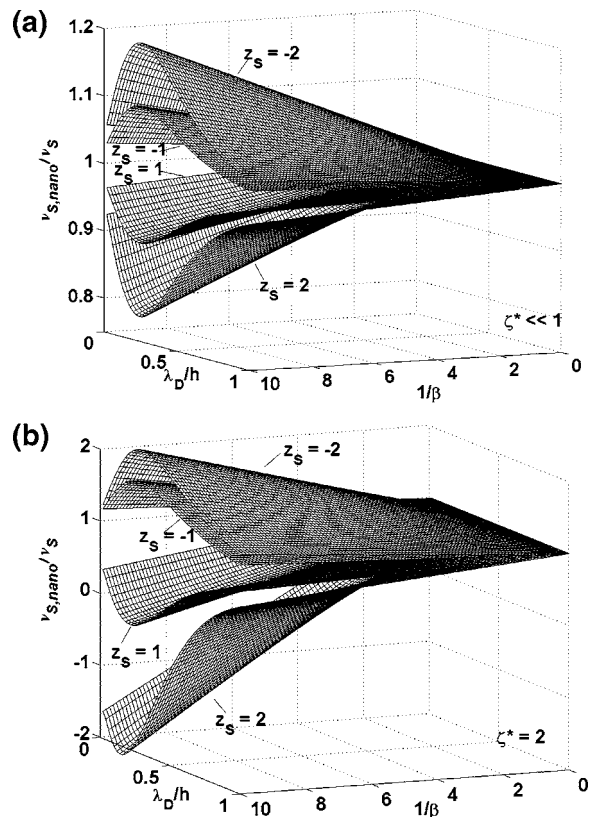


Figure 4. Surface plots of effective electrophoretic mobility in a nanochannel normalized by ion mobility as a function of λ_D/h and $1/\beta$ for (a) $\zeta^* \ll 1$ and (b) $\zeta^* = 2$. Surface plots of $z_S = -2, -1, 1$, and 2 are shown for each case. The separation of $\langle \nu_{S,\text{nano}} \rangle / \nu_S$ surfaces for various values of sample valence, z_S , demonstrates that electrophoresis experiments in nanochannels contain information of both sample valence, z_S , and sample ion mobility, ν_S . Note that, for negative wall charge, positive analytes equilibrate to transverse positions close to the wall and hence experience velocities lower than the area-averaged liquid velocity. Hence, $\langle u_S \rangle$ is less than $\langle u \rangle$ for positive ions and $\langle \nu_{S,\text{nano}} \rangle / \nu_S$ is negative.

solve for the effective electrophoretic mobility of a charged species in nanochannel flow. The ratio of this effective electrophoretic mobility to ion mobility results in a parameter convenient in quantifying the changes of net streamwise electrophoretic flux due solely to finite EDL effects. This ratio also allows us to establish a method whereby both ion valence and mobility may be determined independently from a comparison of micro- and nanoscale transport results.

We first subtract the area-averaged liquid velocity, $\langle u \rangle$, from the observed analyte velocity, $\langle u_S \rangle$, in a nanochannel. We then divide this difference by the electric field and by $z_S F$ to define an “apparent electrophoretic mobility” in a nanochannel: $\langle \nu_{S,\text{nano}} \rangle = (\langle u_S \rangle - \langle u \rangle) / z_S F E$. For a thin EDL channel, this effective mobility reduces to just $\langle \nu_{S,\text{nano}} \rangle = \nu_S$, as expected. The ratio of $\langle \nu_{S,\text{nano}} \rangle$ to ν_S is then

$$\frac{\langle \nu_{S,\text{nano}} \rangle}{\nu_S} = \frac{\langle u_S \rangle - \langle u \rangle}{u_d} = 1 - \frac{1}{\beta} \left(1 - \frac{\psi(y)}{\zeta} \right) \left(\exp \left(\frac{-z_S e (\psi(y) - \psi_c)}{kT} \right) - 1 \right) \quad (23)$$

The minimum number of parameters that determine $\langle \nu_{S,\text{nano}} \rangle / \nu_S$

are β , ζ^* , λ_D/h , and z_S . ζ^* and λ_D/h determine the potential distribution and therefore the shape of the liquid velocity profile. β determines the relative importance of analyte advected by electroosmotic flow and electrophoretic flux. z_S determines the distribution of the sample ion of interest in the potential field determined by the background electrolyte ions.

Figure 4 shows surface plots of $\langle \nu_{S,\text{nano}} \rangle / \nu_S$ versus $1/\beta$ and λ_D/h . The figure is generated using constant values of $\zeta^* \ll 1$ (Figure 4a) and $\zeta^* = 2$ (Figure 4b) and analyte valences, z_S , of 1, 2, -1, and -2. There are three important limits of the $\langle \nu_{S,\text{nano}} \rangle / \nu_S$ parameter. First, at low λ_D/h , the EDL is thin and thus the velocity profile is uniform. In addition, in thin EDL, low Peclet number flow, the species concentration distribution is uniform in the transverse direction. Therefore, the coupling of the streamwise velocity and transverse concentration distribution results in simple area-averaged values for velocity, so $\langle \nu_{S,\text{nano}} \rangle / \nu_S = 1$. Second, $\langle \nu_{S,\text{nano}} \rangle / \nu_S$ approaches unity for high λ_D/h . In this limit, the sample analyte is distributed approximately uniformly over the cross section of the channel and the analyte is simply advected at the area-averaged liquid velocity. Third, at large β , streamwise electromigration velocities are large relative to electroosmotic velocities, thereby resulting in $\langle \nu_{S,\text{nano}} \rangle / \nu_S$ ratios close to unity.

The strongest coupling between finite EDL physics and streamwise transport occurs for intermediate values of λ_D/h and low values of β . At low β , the coupling between the nonuniform flow field and the nonuniform transverse potential (and associated transverse concentration profiles) in the nanochannel govern the transport of analytes. As β increases, the ion mobility of the analyte becomes progressively more important until it dominates axial analyte transport (i.e., until it dominates effective electrophoretic mobility). For an intermediate range of λ_D/h , there is a nonuniform velocity profile covering large portions of the channel cross section. In this regime, transverse electromigration (determined by both $\psi(y)/\zeta$ and z_S) plays a strong role in determining which streamwise velocities are sampled by the analyte. Highly positive analytes (e.g., $z_S = 2$ or greater) reach equilibrium very near the wall and are retarded by the low velocities near the no-slip wall region.

Note the strong asymmetry between positive and negative analytes in the $\zeta^* = 2$ case as compared to the $\zeta^* \ll 1$ case. This asymmetry at high ζ^* is shown clearly in Figure 2 and Figure 4b, and is a result of the nonlinear nature of the EDL. At high ζ^* , the attraction of counterions is more important in determining the EDL potential than the repulsion of co-ions.⁴ For the $\zeta^* \ll 1$ case of Figure 4a, we see that the solutions for $\langle \nu_{S,\text{nano}} \rangle / \nu_S$ are nearly symmetric for both positive and negative ions.

The separation of $\langle \nu_{S,\text{nano}} \rangle / \nu_S$ surfaces for different values of sample valence, z_S , demonstrates an important opportunity offered by nanochannel electrokinetic flows. Electrophoresis experiments in nanochannels contain information regarding both sample valence, z_S , and sample ion mobility, ν_S . A nanochannel measurement can yield streamwise transport dynamics, particularly for an optimal coupling between EDL transverse electromigration to streamwise transport. For the parameters of Figure 4b, the strongest such coupling occurs between $0.3 < \lambda_D/h < 0.5$ and for low values of β . In this regime, there are significant differences between $\langle \nu_{S,\text{nano}} \rangle / \nu_S$ values of different analyte valences. For

example, at $\lambda_D/h = 0.4$, $\zeta^* = 2$, and $\beta = 0.6$ (a condition addressable experimentally³⁵), $\langle \nu_{S,\text{nano}} \rangle / \nu_S$ changes by 15% between $z_S = -1$ to -2 analytes and by 23.5% between $z_S = 1$ and 2 analytes. Given information of ion mobility (i.e., the observable quantity $z_S \nu_S$), a measurement of $\langle \nu_{S,\text{nano}} \rangle$ yields information of species valence.

We define here EKSIV as a process of measuring species velocity in both a microchannel and a nanochannel to yield both ion mobility and valence information. The proposed method is, briefly, as follows: (1) A technique such as current monitoring⁴² or tracking of a neutral marker is used to obtain a measurement of electroosmotic mobility in a thin-EDL microchannel device; (2) the product of species mobility and valence, $z_S \nu_S$, is determined in the same microchannel for a charged analyte (using an empirical value of u_{HS} to subtract out area-averaged liquid velocity from observed analyte velocity); (3) observable species velocity, $\langle u_S \rangle$, and bulk liquid velocity, $\langle u \rangle$, are measured in a nanochannel system of known ζ^* , β , and λ_D/h (for ease of modeling and accuracy, this measurement should be performed under nonoverlapped EDL conditions) and used to determine $\langle \nu_{S,\text{nano}} \rangle$; (4) the model described here is used to generate predictions of the ratio $\langle \nu_{S,\text{nano}} \rangle / \nu_S$; and (5) model predictions are compared to data normalized as per eq 23 to determine the most probable value of valence for each analyte. To improve accuracy, a background electrolyte buffer concentration should be chosen to yield a λ_D/h between 0.3 and 0.5 (i.e., conditions yielding more sensitive dependence of $\langle \nu_{S,\text{nano}} \rangle / \nu_S$ on valence as shown in Figure 4), and β should be minimized to ensure a strong coupling between streamwise and transverse electromigration.

The values of ζ^* , β , and λ_D/h can be appropriately tuned to yield optimal conditions for EKSIV. For example, electroosmotic flow in the nanochannel should not be suppressed, and in many cases, high pH values will allow larger values ζ^* and lower values of β . λ_D/h can be modified using various channel depths or (more conveniently) various values of background electrolyte concentration. Once valence and ion mobility are known, measurements can be used to establish a map of mobility versus valence for each analyte. As these quantities are independent but nonorthogonal parameters, we refer to such a plot as an EKSIV map.

Last, we note that the parameters β and ζ^* all depend on the dimensional value of zeta potential, ζ . In general, ζ is a function of local ionic concentration and pH. In our experiments,³⁵ total ion concentration is conveniently varied to effect variations of λ_D/h (along with limited variations of h). We are therefore forced to simultaneously vary zeta potential as we vary λ_D/h . We can assume a convenient power law for the concentration dependence of zeta potential of the form:³⁹ $\zeta = a c^b$, where c is the ionic species sum, $c = \sum_{i=0}^N z_i c_i$, and a and b are empirical constants. Our measurements³⁵ yield empirical values of $a = 0.298$ and $b = -0.245$. Figure 5 shows example numerical predictions of apparent electrophoretic mobility ratio, $\langle \nu_{S,\text{nano}} \rangle / \nu_S$, as a function of λ_D/h with λ_D/h with $\zeta = 0.288 c^{-0.245}$ (the boundary condition required for $\psi(y)$) and for channel heights of 40, 80, 100, and 120 nm (our experiments are performed in 40- and 100-nm channel depths). Note the coupling between concentration and ζ potential results in multiple solutions for each λ_D/h as changing λ_D also changes ζ potential. In the second of this two-part paper series,³⁵ we will present the results

(42) Sze, A. J. *Colloid Interface Sci.* **2003**, *261*, 402–410.

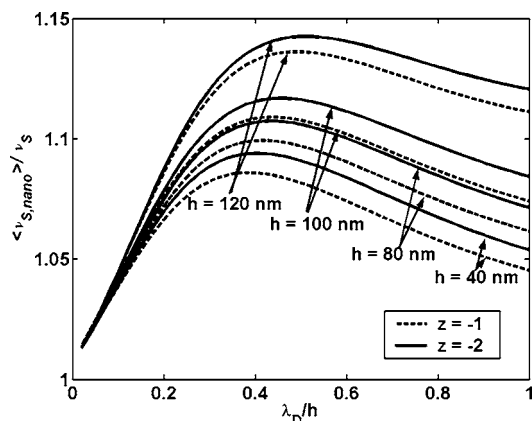


Figure 5. Apparent electrophoretic mobility ratio, $\langle v_{s,\text{nano}} \rangle / v_s$, as a function of λ_D/h with λ_D and ζ coupled by the relation $\zeta = 0.288c^{-0.254}$. Numerical calculations are presented for 40-, 80-, 100-, and 120-nm channels. Values of mobility for the parameter β are taken from the experimentally determined values of mobility for bodipy ($z_s = -1$) and carboxyl fluorescein ($z_s = -2$).

of an experimental parametric study as well as a validation of the current model. This type of theoretical development and comparison with experiments yields insight into the applicability of continuum theory and structure of EDLs in nanoscale electrokinetic systems.

CONCLUSIONS

Nanofluidic systems provide new functionalities for the manipulation of chemical species. In such systems, EDL thicknesses are comparable to characteristic channel dimensions. This finite thickness causes the velocity profile to be highly nonuniform and results in a decrease in area-averaged electroosmotic velocity. In these channels, transverse electromigration and diffusion fluxes are coupled to the streamwise transport of analyte ions. Prior theoretical studies have not addressed this coupling.

We have developed analytical and numerical models for electrokinetic transport in nanometer-scale fluidic channels. The model is valid for the transport of individual charged and uncharged species over long distances (i.e., electrophoresis) and in conditions of both low and high ζ potential. The model considers the addition of dilute analyte sample species to an electrokinetic flow where λ_D is on the order of h . We derive an analytical solution to both the area-averaged (observed) species velocity and the unsteady, streamwise-transverse concentration distributions for both charged and uncharged species. When charged species are introduced into a nanoscale channel with finite double layers, positively charged analyte molecules spend relatively more time near a negatively charged wall and experience lower liquid velocities. Negative sample ions have equilibrium concentration distributions that are more tightly focused near the center of the channel. Transverse electromigration and associated transverse concentration gradients therefore play a critical role in the net streamwise transport of a charged solute in electrokinetic nanochannel flow. The model demonstrates that electrophoretic separation in nanochannels depends on sample ion valence, sample ion mobility, ζ potential, and the Debye length of the background electrolyte. Finally, we propose a new method we term electrokinetic separation by ion valence (EKSIV), where

both valence and mobility of an analyte can be determined from a comparison of microchannel and nanochannel electrophoresis experiments. In the second of this two-paper series, we will present an experimental validation of the model as well as a demonstration of EKSIV.

ACKNOWLEDGMENT

This work is sponsored by the National Institutes of Health (Grant N01-HV-28183) and by a National Science Foundation PECASE Award (J.G.S., CTS-0239080-001) with Dr. Michael W. Plesniak as grant monitor.

GLOSSARY

a	radius of cylindrical nanochannel (m)
c_i	concentration of species i (mol)
c	sum over all species concentrations, $\sum_{i=1}^N c_i$ (mol)
$\langle c \rangle$	area-averaged concentration (mol)
D	molecular diffusion coefficient ($\text{m}^2 \text{s}^{-1}$)
e	elementary charge (C)
E	electric field strength (V m^{-1})
F	Faraday's constant (C mol^{-1})
h	transverse half-height for a rectangular cross-section channel (m)
k	Boltzmann's constant (J K^{-1})
n_c	number density (m^{-3})
n_o	number of moles (mol)
T	temperature (K)
t	time (s)
\bar{u}	liquid velocity field (m s^{-1})
$\langle u \rangle$	area averaged (bulk) liquid velocity (m s^{-1})
u_d	species drift velocity, $v_s z_s F E$ (m s^{-1})
u_{HS}	Helmholtz–Smoluchowski velocity $\epsilon \zeta E / \mu$
u_s	observed species velocity (m s^{-1})
$\langle u_s \rangle$	area-averaged observed species velocity (m s^{-1})
w	channel width (m)
z	valence number
β	ratio of ion drift velocity to Helmholtz–Smoluchowski velocity, $\mu v_s z_s F / \epsilon \zeta$
ϵ	permittivity ($\text{C}^2 \text{J}^{-1} \text{m}^{-1}$)
κ_s	surface conductivity (S/m)
μ	dynamic viscosity (Pa s)
v_s	ion mobility of species s (mol s kg^{-1}), $u_d / z_s F E$
$\langle v_{s,\text{nano}} \rangle$	electrophoretic mobility in nanochannel, $(\langle u_s \rangle - \langle u \rangle) / z_s F E$ (mol s kg^{-1})
λ_D	Debye length (m^{-1})
ρ_e	volumetric charge density (C m^{-3})
ϕ	potential applied via end-channel electrodes (V)
ψ	potential associated with wall charges (V)
σ	conductivity (S m^{-1})
Φ	total electric potential (V)
ζ	zeta potential (V)
ζ^*	nondimensional zeta potential, $ze\zeta/kT$

Subscripts

A	background electrolyte cation
B	background electrolyte anion
c	centerline
S	sample ion
adv	advection
cyl	cylindrical
diff	diffusion
em	electromigration
HS	Helmoltz–Smolchowski
nano	nanometer scale (implying finite electric double layers)

APPENDIX A: CYLINDRICAL GEOMETRY NANOCHANNELS

The extension of the model to cylindrical coordinates is trivial. Consider a cylindrical tube of radius a with radial and streamwise coordinates r and x , respectively. The area-averaged velocity of the analyte is given by eq 4 with $\psi(y,z)$ replaced by $\psi(r)$. For low ζ potential, the Debye–Huckel approximation yields a radial velocity profile, $u(r)$,⁷ equal to $-(\epsilon E \zeta / \mu) [1 - I_0(r/\lambda_D) / I_0(a/\lambda_D)]$, where I_0 is the zero-order modified Bessel function of the first kind. Following the derivation from our continuum theory section, we then integrate the balance between radial diffusion and radial electromigration to yield an expression for the unsteady streamwise-radial concentration distribution, $c_S(r,t)$, which has the same form of eq 15 with the coordinate y replaced by r . The closed form analytical solution for the species velocity in a cylindrical nanochannel, $\langle u_{S,cyl} \rangle$ is then given by eq 19 (again with y replaced by r). For the cylindrical case, the area averaging operator is understood to be $\langle \rangle = 2/(\pi a^2) \int_0^a (\) r dr$.

Combining the results for a cylindrical geometry, the streamwise-radial concentration distribution is

$$c_S(x,r,t) = \frac{n_0}{\pi a^2} \frac{\exp(-(x - \langle u_S \rangle t)^2 / 4Dt)}{\sqrt{4\pi Dt}} \times \exp\left(\frac{-z_S e(\psi(r) - \psi_c)}{kT}\right) \quad (24)$$

For low ζ potential, this concentration distribution becomes

$$c_S(x,r,t) = \frac{n_0}{\pi a^2} \frac{\exp(-(x - \langle u_S \rangle t)^2 / 4Dt)}{\sqrt{4\pi Dt}} \times \exp\left(\frac{-z_S e(I_0(r/\lambda_D))}{kT(I_0(a/\lambda_D))}\right) \quad (25)$$

And finally, the ratio of $\langle v_{S,nano} \rangle$ to ion mobility v_S is

$$\frac{\langle v_{S,nano} \rangle}{\langle v_S \rangle} = 1 - \frac{1}{\beta} \left(\left(1 - \frac{\psi(r)}{\zeta} \right) \left(\exp\left(\frac{-z_S e(\psi(r) - \psi_c)}{kT}\right) - 1 \right) \right) \quad (26)$$

The analysis presented here can also be applied to a variety of other cross sections by leveraging analytical or numerical expressions, or both, for the potential and velocity fields.

Received for review May 13, 2005. Accepted August 19, 2005.

AC050835Y